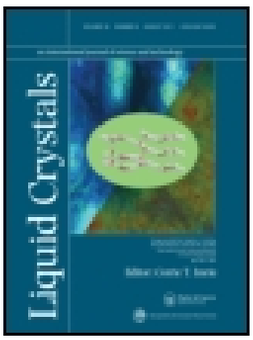

Liquid Crystals

ISSN: 0267-8292 (Print) 1366-5855 (Online) Journal homepage: http://www.tandfonline.com/loi/tlct20

Travelling fingers in two-frequency cholesteric liquid crystals: fragments, loops and spirals

S. Pirkl & P. Oswald

To cite this article: S. Pirkl & P. Oswald (2001) Travelling fingers in two-frequency cholesteric liquid crystals: fragments, loops and spirals, Liquid Crystals, 28:2, 299-306, DOI: 10.1080/02678290010007233

To link to this article: http://dx.doi.org/10.1080/02678290010007233

Published online: 06 Aug 2010.

LIQUID CRYSTALS, 2001, VOL. 28, NO. 2, 299–306

Travelling fingers in two-frequency cholesteric liquid crystals: fragments, loops and spirals

S. PIRKL* and P. OSWALD

Laboratoire de Physique de l'Ecole Normale Supérieure de Lyon, CNRS, UMR 8514, 46 Allée d'Italie, 69364 Lyon Cedex 07, France

(*Received 14 April 2000; in final form 27 July 2000; accepted 25 August 2000*)

We review the different dynamical patterns that cholesteric fingers of the first type (CF-1) and of the second type (CF-2) form in an a.c. electric field near the coexistence line with the homeotropic nematic phase. Videomicroscopy and computer image analysis were used for investigation of the patterns in polarized light. We show that CF-1s can form stable rectilinear fragments that crawl at constant velocity along their axes, whereas CF-2s form only unstable curved fragments that drift perpendicularly to their axes. Observations of CF-2 staple-shaped fragments which continuously lengthen in their centres are also reported. Finally, we describe in detail the experimental conditions in which CF-2 loops and spirals grow, collapse and destabilize.

1. Introduction

It has long been known that the helical structure of a cholesteric phase can be unwound by confining the sample between two glass electrodes treated for homeotropic anchoring [1, 2]. The nematic phase forms when the confinement ratio between the sample thickness and the equilibrium pitch ($C = d/p$ where d is the sample thickness and p the equilibrium cholesteric pitch) is typically less than 1. At a larger confinement ratio, the cholesteric phase can still be unwound by applying an electric field, provided that the liquid crystal is of positive dielectric anisotropy $\Delta\varepsilon$ [3, 4]. This bifurcation is usually subcritical [5] and typical textures are composed of cholesteric fingers that spontaneously form near the coexistence line between the two phases. Different types of cholesteric fingers can nucleate [6], with very different static and dynamical properties.

The cholesteric fingers of the first type (or CF-1) are the most common [1–8]. Their director field is continuous. A segment of a CF-1 spontaneously collapses above the coexistence line (at high voltage or small thickness) whereas it lengthens from its two ends while undulating below. The two ends of a CF-1 segment are different [3, 9]). As a result, a segment of a CF-1 can 'crawl' along its axis in an a.c. electric field, which was indeed observed experimentally in the conducting regime [10].

Cholesteric fingers of the second type or CF-2 [10–13] differ from the CF-1s in many respects. A CF-2 segment has a point defect at each end [14] and may form a cholesteric bubble when shortening [15, 16]. The CF-2s can also drift perpendicularly to their axes in an a.c. electric field and form growing loops or spirals [14]. These solutions have already been described in many articles, but the precise conditions under which they form have not yet been systematically described. The motion of both fingers is clearly due to an electrohydrodynamical coupling between the electric field, the charges and the director field inside the finger [11], but a theoretical model is still missing.

Our purpose in this article is to specify better the experimental conditions and the values of the control parameters for which the different solutions (spiral, loop, etc.) develop. In addition, we will pay special attention to a new class of solutions that are the stationary fragments of a CF-1 and of a CF-2. The plan of the article is as follows. In the next section we give the experimental procedure and explain the choice for working with two-frequency mixtures instead of more conventional systems. In the following sections we describe the different solutions: the straight CF-1 fragments (§ 3), the CF-2 loops (§ 4), the curved and 'staple-shaped' CF-2 fragments (§ 5 and 6) and the spirals (§ 7). Our results are then summarized in § 8.

2. Experimental

For greater convenience, we used two-frequency mixtures of nematic liquid crystals ZLI 2979 (from E. Merck) [17] and Roche 3421 (from Hoffman-La Roche). In these mixtures, the dielectric anisotropy $\Delta\varepsilon$ vanishes and changes sign above some cut-off frequency f_o, i.e. $\Delta\varepsilon > 0$

* Author for correspondence. Permanent address: University of Pardubice, Department of Physics, 53210 Pardubice, Czech Republic; e-mail: slavomir.pirkl@upce.cz

Liquid Crystals ISSN 0267-8292 print/ISSN 1366-5855 online © 2001 Taylor & Francis Ltd
http://www.tandf.co.uk/journals
DOI: 10.1080/02678290010007233

at $f < f_o$ whereas $\Delta\varepsilon < 0$ at $f > f_o$. Catalogue parameters at room temperature and our estimates of $\Delta\varepsilon_L$ and f_o at 30 and 50°C for the basic mixtures are listed in table 1.

In order to accelerate finger dynamics, which are very slow at room temperature, experiments were systematically performed at 30°C for the Merck mixture and at 50°C for the Roche mixture. To obtain cholesteric phases we added small quantities of chiral ZLI 811 (from E. Merck) to the above mixtures. The equilibrium pitches were measured using the conventional Cano wedge method and are given in table 2 for three different concentrations.

Another reason for working with these mixtures is that they allow us to obtain CF-2 fingers very easily from the cholesteric bubbles by manipulating the voltage [17]. Note that bubbles are always very numerous in the sample [16]. Moreover, the fingers move much faster in these mixtures than in conventional systems composed only of molecules with positive dielectric anisotropy; this makes the observation of their dynamics much easier. A square-wave voltage of frequency $f \ll f_o$ is used, so that the dielectric anisotropy is equal to $\Delta\varepsilon_L$ given in table 1. We also systematically worked in the conducting regime, i.e. at smaller frequency than the charge relaxation frequency f_c of the samples. This is important because the fingers move only in this regime. Moreover, we know from previous experiments that at low frequency ($f \ll f_c$) their velocity is independent of the frequency and of the conductivity of the samples [6, 11]. The charge relaxation frequency f_c is obtained by measuring with a precision LCR meter HP 4284A the complex impedance $R + iX$ of the samples as a function of the frequency. We typically found $f_c \approx 2$ kHz for Merck samples at 30°C and $f_c \approx 15$–18 kHz for Roche samples at 50°C. The samples were prepared between two parallel electrodes (ITO) coated with a silane to obtain a strong homeotropic anchoring. Nickel wires of calibrated diameters were used to fix the thickness d of the samples. In the following, the dimensionless confinement ratio is defined to be $C = d/p$. This parameter and the applied voltage V are the two control parameters of the experiment.

All observations and measurements were performed using a polarizing microscope equipped with a video camera, a colour monitor, a video cassette recorder, and a video copy processor. For measurements on the pictures we used a PC computer and the image processing software LUCIA (LIM, Prague).

The phase diagram of the chiralized mixture ZLI 2979 in an a.c. electric field is given in [18] at both low frequency ($f = 100$ Hz; $\Delta\varepsilon > 0$) and high frequency (30 kHz; $\Delta\varepsilon < 0$). In this work we restrict ourselves to the low frequency regime ($\Delta\varepsilon > 0$). Typical values of the characteristic voltages entering into the problem are given in table 2. We recall here that V_0 is the voltage below which the nematic phase becomes unstable (spinodal limit of the nematic phase); V_2 is the coexistence voltage between the CF-1s and the homeotropic nematic phase (see also § 3); V_3 defines the spinodal limit for the CF-1s. Other voltages are defined in the following sections.

Table 1. Properties of commercial nematic mixtures. T_{NI} is the nematic–isotropic transition temperature, Δn the optical birefringence, $\Delta\varepsilon_L$ (resp. $\Delta\varepsilon_H$) the dielectric anisotropy at low (resp. high) frequency and f_0 the frequency at which $\Delta\varepsilon$ vanishes.

Basic mixture	T_{NI}/°C	Δn	$\Delta\varepsilon_L$	$\Delta\varepsilon_H$	f_0/kHz	T/°C
ZLI	126	0.122	+ 2.0	− 1.2	2.0	20
2979			≈ + 2		≈ 5.0	30
Roche	78	1.105	+ 4.4	− 4.35	1.4	22
3421			≈ + 3.8		≈ 35	50

3. CF-1 fragments

We first recall known results and definitions. We know from previous experiments that there exists a voltage V_2 at which the long fragments of a CF-1 (long means that their length is much larger than p) crawl along their axes while keeping a constant length [10]. Their two tips thus move with opposite velocities, i.e. $v_{(\text{rounded tip})} = -v_{(\text{pointed tip})}$. This voltage defines the coexistence line between the CF-1s and the nematic phase (their relative

Table 2. Cholesteric pitch p and characteristic voltages measured at $f = 100$ Hz and $T = 30$°C for the Merck mixture and at $f = 2$ kHz and $T = 50$°C for the Roche mixtures. Voltages (see the text) are given in V_{rms}. For V_2^* we give the typical values measured from 50–60 μm long fragments. They are very close to V_{2-}^* (see the text). V_{sb} is the voltage above which the cholesteric bubbles spontaneously disappear.

Basic mixture	ZLI 811/wt %	p/μm	$C = d/p$	V_0	V_2	V_{2+}	V_{2+}^*	V_{rtr}^*	V_{tr}^*	V_3	V_{sb}
ZLI 2979	0.615	16.05	1.56	2.60	6.19	6.59	6.29			12.50	9.55
ROCHE 3421	0.64	15.55	1.93	2.92	5.29	5.45	5.30	7.6	8.30	8.05	6.98
ROCHE 3421	1.25	7.45	4.02	5.85	11.73	11.77	11.75	12.2	14.55	14.55	13.4

proportions remain invariant in time). An alternative definition for V_2 is that it is the voltage below which a very long finger spontaneously starts to undulate, because it becomes energetically better than the surrounding nematic phase. In practice, these two criteria give very similar values for V_2 and cannot be distinguished within the experimental errors (of the order of 10^{-2} V). Another important property of the CF-1s is that they never drift perpendicularly to their axes in an a.c. electric field. This is a direct consequence of their invariance by a rotation of π around their axes 19].

We now report new observations in the two-frequency mixtures. We observed that above V_2 long fragments of a CF-1 shorten, but do not systematically collapse as in ordinary mixtures. On the contrary, they stop shortening (see figure 1) when they have reached a characteristic length $L(V)$ that depends only on the voltage, and then propagate at a constant velocity along their axes (see figure 2). Nevertheless they collapse above a typical voltage $V_{2+} > V_2$ that is given in table 2. We emphasize that these fragments are stable between V_2 and V_{2+}, shortening when they are too long and lengthening when they are too short. These solutions appear to be specific for the two-frequency mixtures and have never been observed in cyanobiphenyls and other mixtures composed of molecules of positive dielectric anisotropy only. We also note that they are more difficult to observe in thick samples ($C > 3$).

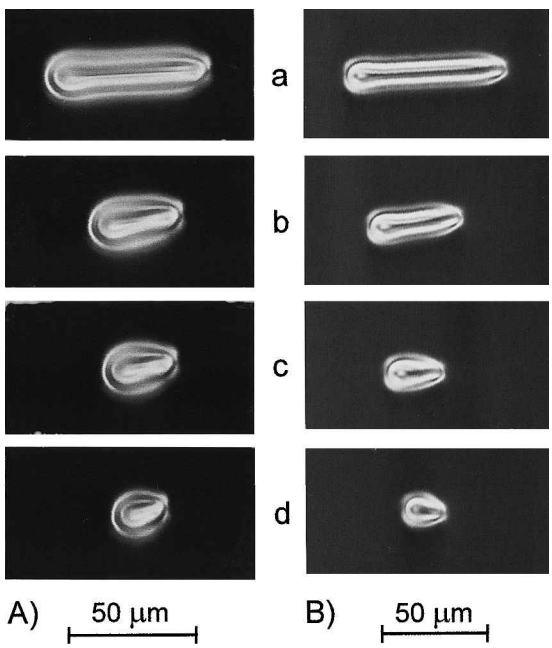

Figure 1. CF-1 fragments observed between crossed polarizers at different voltages. (A) Merck mixture at $C = 1.56$, $d = 25\,\mu m$, $f = 100\,Hz$ and $T = 30°C$: (*a*) $V = V_2 = 6.195$ V, (*b*) $V = 6.200$ V, (c) $V = 6.300$ V, (*d*) $V = 6.590$ V. (B) Roche mixture at $C = 1.93$, $d = 30\,\mu m$, $f = 2\,kHz$ and $T = 50°C$. (*a*) $V = V_2 = 5.192$ V, (*b*) $V = 5.210$ V (*c*) $V = 5.220$ V, (*d*) $V = 5.339$ V. Photographs 1(*a*), 1(*b*), 1(*c*),... correspond to curves in figure 2.

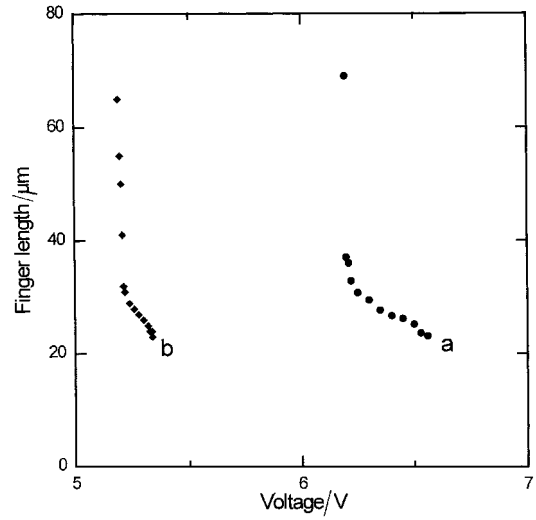

Figure 2. Length L of the CF-1 fragments as a function of the voltage V. L diverges when $V \to V_2$. By convention, velocity v is positive when the finger moves from the rounded tip to the sharp one. See also figure 1. (*a*) Merck mixture at $T = 30°C$ and $C = 1.56$, $d = 25\,\mu m$ and $f = 100\,Hz$; (*b*) Roche mixture at $T = 50°C$, $C = 1.93$, $d = 30\,\mu m$ and $f = 2\,kHz$.

4. CF-2 loops

These solutions have been recently observed in normal cholesterics with positive dielectric anisotropy [14]. They are impossible to make in thin samples ($C < 2$–3). By contrast, they spontaneously form in thick samples ($C > 3$) from the electric field-induced homeotropic nematic phase after switching the voltage below V_0.

Another recent observation is that the CF-2s get thinner above some voltage V_{tr}^* that is very close to the spinodal limit V_3 for CF-1 [14] (see figure 3). This transformation usually occurs a few seconds after the voltage has been changed and runs from dust particles or anchoring defects on the electrodes. The transformation is slower in two-frequency mixtures than in previously investigated mixtures of cyanobiphenyls, and is strongly hysteretic. Indeed, the voltage must be decreased below a voltage V_{rtr}^* that is typically 2 V below V_{tr}^* in order that the finger recovers its initial width. Experimental values of V_{rtr}^* and V_{tr}^* are given in table 2.

We also observed that, as in usual systems, loops before transformation can grow or collapse depending on their initial radius [14] (see figure 4). There exists therefore, for each value of the voltage, a critical radius R_c. In principle, the situation is similar with transformed loops above V_{tr}^* but their critical radius is so large (more than 500 μm) that in practice it is almost impossible

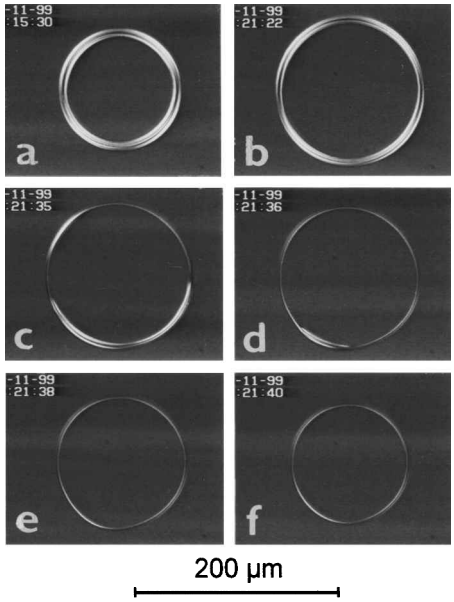

Figure 3. Loop of a CF-2 in the Roche mixture at $C = 4.02$, $d = 30\,\mu m$ and $f = 2\,kHz$ before the transformation at $V = 12\,V$ and $t = 0\,s$ (*a*) and after switching the voltage to $V = 14.65\,V$ ($V^*_{tr} = 14.62\,V$) at $t = 352\,s$ (*b*), $t = 365\,s$ (*c*), $t = 366\,s$ (*d*), $t = 368\,s$ (*e*) and $t = 370\,s$ (*f*). Crossed polarizers.

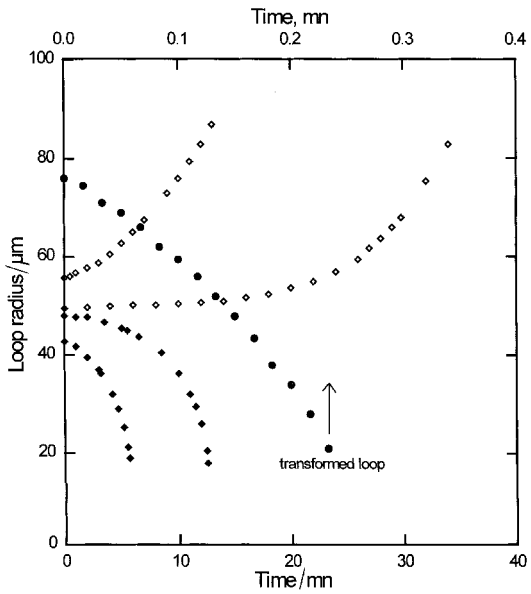

Figure 4. (*a*) Loop radius versus time at $V = 14\,V$ for the same loop as in figure 3. The loop grows or collapses depending on its initial radius. In this example the critical radius is close to $R_c = 47.5\,\mu m$. (*b*) Collapse of the transformed loop after transformation at $V = 14.65\,V$ (critical radius $R_c > 500\,\mu m$) (see upper time scale in the graph).

to measure. The critical radius as a function of voltage fits quite well to a linear law as long as R_c is large in comparison with the finger width (see figure 5). We

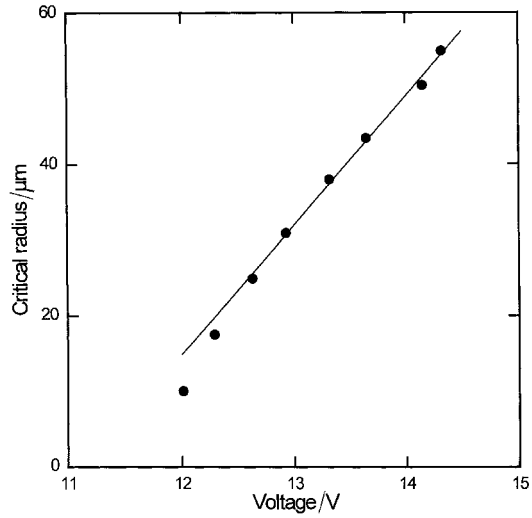

Figure 5. Critical radius of non-transformed loops as a function of voltage for the Roche mixture at $C = 4.02$, $f = 2\,kHz$ ($V^*_2 = 11.75\,V$, $V_u \approx 11.65\,V$ and $V^*_{tr} = 14.55\,V$).

found that the linear fit extrapolates to some voltage that is close to the voltage V_u below which loops of very large diameter (or linear fingers) are unstable with respect to spontaneous undulation. It is worth noting that in two-frequency mixtures V_u is significantly smaller than the voltage V^*_2 at which CF-2 fragments of constant length propagate (see the next section). For instance, $V_u \approx V^*_2 - 0.2\,V$ for the Roche mixture, whereas in ordinary systems these two voltages are the same (within $10^{-2}\,V$). This difference between V_u and V^*_2 has direct consequences on the dynamics of the spirals that will be discussed in § 7.

5. CF-2 fragments

In thin samples, CF-2s do not form spontaneously from the nematic phase after decreasing the voltage. One way of obtaining a CF-2 fragment is to stretch a cholesteric bubble by decreasing the voltage below V_s. In practice V_s is smaller than the coexistence voltage V_2 (typically 0.2 V below V_2 in the Roche mixture and 0.6 V below V_2 in the Merck mixture). In this way two CF-1 segments with two rounded ends start to grow from the bubble which then splits to give a CF-2 segment embedded in a CF-1 finger (see figure 6). An important point is that the CF-2 segment is energetically more favourable than the CF-1 at all voltages and systematically lengthens inside the CF-1. The lengthening velocity of the CF-2 as a function of the applied voltage is given in figure 7.

It is also very well known that CF-2s (contrary to CF-1s) drift perpendicularly to their axis and do not crawl along their axes in an a.c. electric field. This is due to their symmetry properties [14, 19].

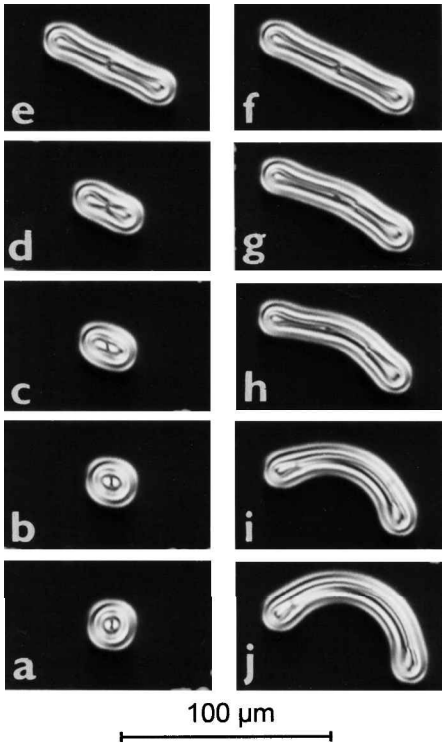

Figure 6. Nucleation and growth of a CF-2 segment by splitting of a cholesteric bubble in the mixture Roche 3421 at 50°C. $C = 1.93$, $d = 30\,\mu m$, $f = 2\,kHz$. (*a*) $V = 5.06$ V; (*b*) $V = 5.03$ V, $t = 0$; (*c*) $V = 5.03$ V, $t = 10$ s; (*d*) $V = 5.03$ V, $t = 14$ s; (*e*) $V = 5.03$ V, $t = 27$ s; (*f*) $V = V_2 = 5.25$ V, $t = 76$ s; (*g*) $V = 5.25$ V, $t = 155$ s; (*h*) $V = 5.25$ V, $t = 176$ s; (*i*) $V = 5.25$ V, $t = 219$ s; (*j*) $V = 5.25$ V, $t = 280$ s. Crossed polarizers.

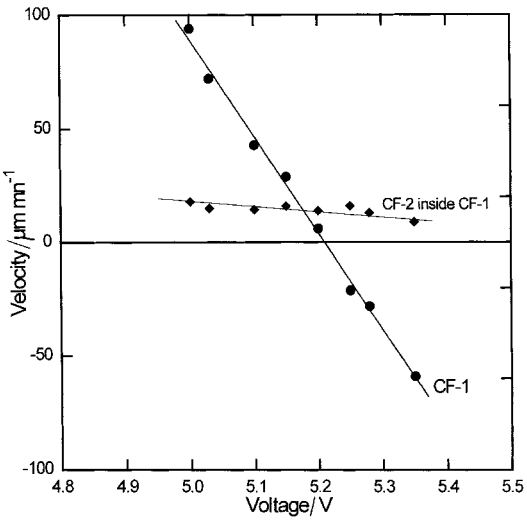

Figure 7. Velocity of the end of a CF-2 segment embedded in a CF-1 fragment (see figure 6) and velocity of the CF-1 rounded tip versus voltage. Mixture Roche 3421 at $C = 1.93$, $d = 30\,\mu m$, $f = 2\,kHz$ and $T = 50°C$.

In a previous publication [17], we mentioned that for some voltage V_2^*, CF-2s can form finite fragments, that drift perpendicularly to their axes while keeping a constant length. We made more systematic observations on these solutions and found that V_2^* slightly depends on the length of the fragment (see figure 8). More precisely, there are minimal and maximal lengths, and minimal and maximal voltages (V_{2-}^* and V_{2+}^*), between which it is possible to observe these solutions. Thus, below V_{2-}^* the finger always lengthens whatever its initial length and can give a spiral. The centre of the spiral then describes a closed trajectory (a circle) as shown in section 7. We observed that at voltage V_{2+}^* the fragment is a little shorter than half a circle, see figure 9 (*d*). Above V_{2+}^*, there is a critical length (which depends on the

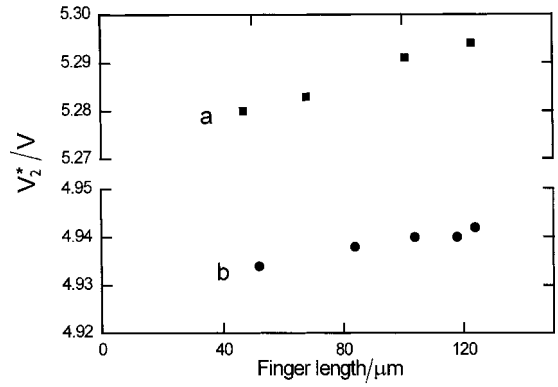

Figure 8. Critical voltage V_2^* as a function of the length of the CF-2 fragment in the Roche mixture at 50°C. (*a*) $C = 1.93$, $d = 30\,\mu m$, $f = 2\,kHz$; (*b*) $C = 1.93$, $d = 30\,\mu m$, $f = 50\,Hz$.

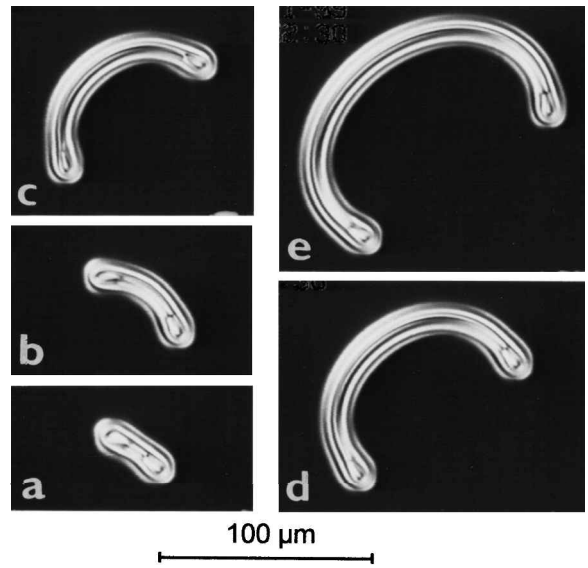

Figure 9. Fragments of a CF-2 observed in the Roche mixture at $T = 50°C$, $C = 1.93$, $d = 30\,\mu m$, $f = 2\,kHz$. Crossed polarizers. (*a*) $V = 5.280$ V, (*b*) $V = 5.283$ V, (*c*) $V = 5.294$ V, (*d*) $V = 5.264$ V, (*e*) $V = 5.266$ V.

voltage) below which the fragment shortens to give a bubble, and above which it lengthens to give a spiral. The inner tip of the spiral then describes an open trajectory as shown in section 7.

We emphasize that fragments, although observable over a very long time, are unstable (and so are transient solutions): indeed, for a given voltage $V_2^{*}{}_- < V < V_2^{*}{}_+$ a too short fragment shortens, whereas a too long one lengthens. This means that, even in this range of voltages, other solutions (like spirals) may exist.

A more surprising observation is that the drift velocity of a fragment strongly depends on its length (and shape) and passes through a maximum for some intermediate length (see figure 10). At the maximum, the fragment resembles an arc of a circle of total length nearly 1/3 of the perimeter of the circle, see figure 9 (*c*). Note that short fragments drift more slowly than spiral arms, whereas long ones go faster.

6. Staple-shaped CF-2

This peculiar solution is observed just below $V_2^{*}{}_-$ and systematically develops from usual short arched segments similar to those shown in figure 9 (*a*). The solution is not stationary and changes shape continuously (see figure 11). More precisely, the finger looks like a staple with a central part that continuously lengthens and flattens, while its two hooked ends remain similar and move away from each other.

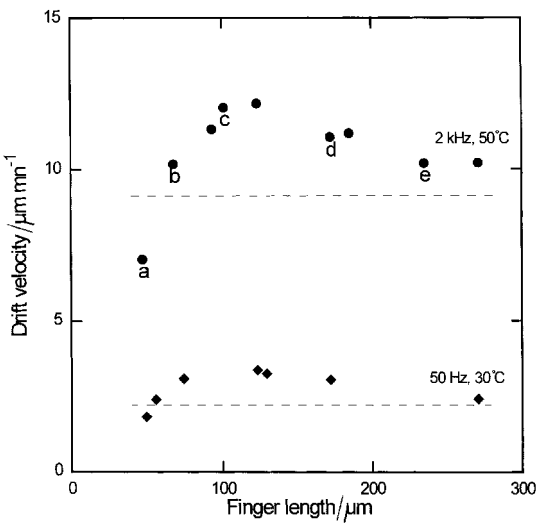

Figure 10. Drift velocity as a function of the length of the CF-2 fragment at $C = 1{,}93$ in the Roche mixture for two different frequencies and temperatures. The dotted lines give the asymptotic drift velocity of a CF-2 in a spiral far from its centre. Points $a, b, c \ldots$ on the curve at $T = 50°C$ correspond to photographs 9 (*a*), 9 (*b*), 9 (*c*).

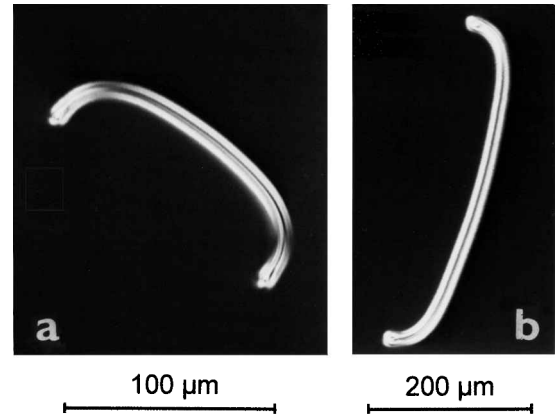

Figure 11. Staple-shaped CF-2 in mixture Roche 3421 at 50°C. Crossed polarizers. (*a*) $C = 4.02$, $d = 30\,\mu m$, $V = 11.72$ V, $f = 2$ kHz; (*b*) $C = 1.93$, $d = 30\,\mu m$, $V = 5.263$ V, $f = 2$ kHz.

7. Spirals

Although these solutions have been studied in many publications [6, 10, 12, 13, 17], a few comments about the different solutions are worth noting. Two types of single spirals are frequently observed: with one end attached to a dust particle or with two free ends.

The former form at all voltages provided that the fingers are long enough and we wait long enough. The spirals then resemble rotating Archimedian spirals with their outer tips describing open trajectories. We emphasize that the spiral is an attractor for any solution to this problem.

The latter are qualitatively different, depending on the voltage. Indeed, below some voltage V_x (close to V_2 and a little bit smaller than V_2^{*}) and above V_n (below this voltage, which is a little larger than V_u, CF-1 segments start to grow from the two ends of the CF-2), the single spirals tend to lengthen from their two ends. In this case, their inner tips describe circles of finite radii with a constant velocity, while their outer tips describe logarithmic spirals, see figure 12 (*a*). By contrast, we observe that the trajectories of the two tips are open above V_x and resemble almost straight lines at V_x—at this voltage, the tangential tip velocity $v_t \approx 0$, see figure 12 (*b*). Above V_x the total length of the spirals increases in time in spite of the fact that the fingers generally shorten from their two ends. Another consequence of the competition between the global lengthening of the spiral (due to its drift) and its shortening from its two ends is that the surface area of the homeotropic nematic region in the centre of the spiral continuously increases.

Finally, twin spirals can also be observed. We note that they form preferentially from fragments close V_2^{*} whereas single ones are much easier to make from fragments close to V_n.

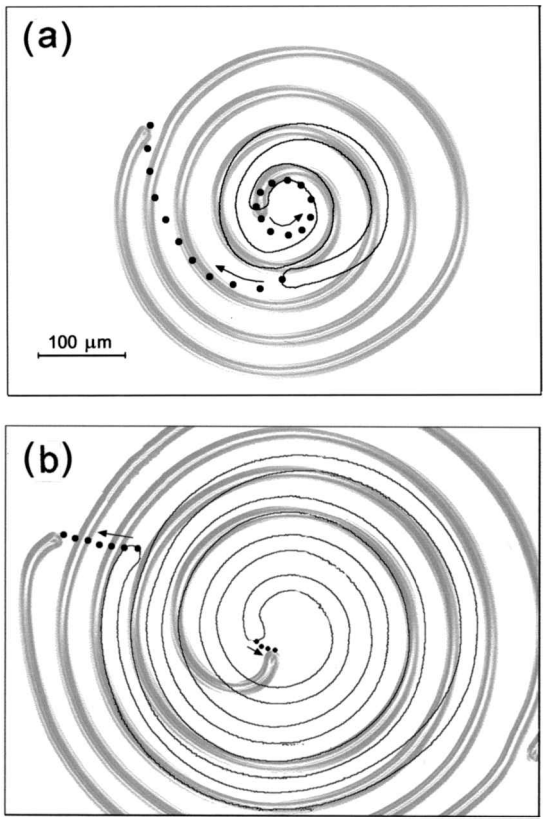

Figure 12. Single spirals in the Roche mixture at $C = 1.93$, $d = 30\,\mu m$, $T = 50°C$ and different voltages ($V_{2-}^{*} = 5.264$ V, $V_2 = 5{,}25$ V). (*a*) $V = 5.144$ V; the inner tip describes a circle (at angular velocity $73° \text{ min}^{-1}$) and the outer tip a logarithmic spiral. Outline $t = 0$ min, shadow sketch $t = 10$ min. (*b*) $V = 5.24$ V; both tips describe an open trajectory. Outline $t = 0$ min, shadow sketch $t = 9$ min. Dots on the photographs show the tip trajectories.

8. Conclusion

Experiments show that for each value of the confinement ratio (providing that C is larger than $K_3/2K_2$, where K_3 and K_2 are the bend and the twist modulis, respectively, in order that the cholesteric fingers develop at zero electric field), there exist characteristic voltages that delimit the different growth modes of the fingers.

For the CF-1s, we observe that: (1) for $V < V_2$ the fingers continually lengthen while they undulate and crawl along their axes; (2) for $V_2 < V < V_{2+}$ the fingers form stable rectilinear fragments of finite length and crawl at constant velocity; (3) for $V_{2+} < V < V_3$ the fingers shorten and collapse (they 'melt' from their two ends and the amplitude of their undulations decreases); (4) for $V > V_3$, the fingers are absolutely unstable and spontaneously break along their axes.

We recall that there exists a voltage $V_1 < V_2$ below which isolated fingers are unstable and continuously split from their rounded ends, forming flower-like patterns.

For the CF-2s, the situation is more complicated and can be summed up as follows. (1) For $V < V_2^{*}$, the fingers lengthen while drifting. They can exist as circular loops or as single or twin spirals. Twin spirals form preferentially close to V_2^{*} and single ones close to V_n ($< V_2^{*}$). Below V_n, CF-1 segments grow from both free ends of the spirals and disturb them, while below V_u ($< V_n$), loops and spirals spontaneously undulate. (2) For $V_{2-}^{*} < V < V_{2+}^{*}$ fragments of constant lengths drift at constant velocities. These solutions are unstable, forming bubbles if shortening and spirals if lengthening. We note that the fingers can form staple-shaped fragments that continuously lengthen in their centre very near V_{2-}^{*}. (3) For $V > V_2^{*}$ the fingers locally shorten from their two ends, but drift, and so can globally lengthen and form spirals if they are long enough. They can also form circular loops but there exists now a critical radius above which they grow and below which they shrink. (4) For $V > V_{tr}^{*} \approx V_3$ the fingers get abruptly thinner but do not break like the CF-1s. They shorten so rapidly from their two ends (when open) that spirals always disappear (they are never long enough). Transformed finger loops can grow or collapse depending on their initial radius, but their critical radius is much larger than before transformation. (5) Finally we note the existence of a voltage $V_s \approx V_u$ below which cholesteric bubbles split.

This work was supported by the European Research Network 'Pattern Noise and Chaos in Complex Systems' under Contract No. FMRX-CT96-0085, by the Czech Grant Agency under Contract No. 202/99/1120; and by the Barrande Program between France and the Czech Republic under Contract No. 98010. We thank Jean Baudry for helpful discussions.

References

[1] (*a*) Brehm, M., Finkelmann, H., and Stegemeyer, H., 1974, *Ber. Bunsenges. phys. Chem.*, **78,** 883; (*b*) Harvey, T., 1978, *Mol. Cryst. liq. Cryst.*, **34,** 224.
[2] Press, M. J., and Arrott, A. S., 1976, *J. Phys. Paris*, **37,** 387.
[3] Ribière, P., and Oswald, P., 1990, *J. Phys. Fr.*, **51,** 1703.
[4] Ribière, P., Pirkl, S., and Oswald, P., 1991, *Phys. Rev. A*, **44,** 8198.
[5] Lequeux, F., Oswald, P., and Bechhoefer, J., 1989, *Phys. Rev. A*, **40,** 3974.
[6] Baudry, J., 1999, PhD thesis, Ecole Normale Supérieure de Lyon, France.
[7] Pirkl, S., 1991, *Cryst. Res. Technol.*, **26,** K111.
[8] Nagaya, T., Hikita, Y., Orihara, H., and Ishibashi, Y., 1996, *J. phys. Soc. Jpn.*, **65,** 2713.
[9] Stieb, A., 1980, *J. Phys. Fr.*, **41,** 961.
[10] Ribière, P., Oswald, P., and Pirkl, S., 1994, *J. Phys. II Fr.*, **4,** 127.

[11] Baudry, J., Pirkl, S., and Oswald, P., 1999, *Phys. Rev. E*, **60,** 2990.
[12] (*a*) Gilli, J. M., and Kamayè, M., 1992, *Liq. Cryst*., **11,** 791; (*b*) Gilli, J. M., and Kamayè, M., 1992, *Liq. Cryst*., **12,** 545.
[13] (*a*) Mitov, P., and Sixou, P., 1992, *J. Phys. II Fr*., **2,** 791; (*b*) Mitov, P., and Sixou, P., 1993, *Mol. Cryst. liq. Cryst*., **231,** 11.
[14] Baudry, J., Pirkl, S., and Oswald, P., 1999, *Phys. Rev. E*, **59,** 5562.
[15] Kawachi, M., Kogure, O., and Kato, Y., 1974, *Jpn. J. appl. Phys*., **13,** 1457.
[16] Pirkl, S., Ribière, P., and Oswald, P., 1993, *Liq. Cryst*., **13,** 413.
[17] Pirkl, S., and Oswald, P., 1996, *J. Phys. II Fr*., **6,** 355.
[18] Pirkl, S., 1994, *Liq. Cryst*., **16,** 973.
[19] (*a*) Gil, L., and Thiberge, S., 1997, *J. Phys. II Fr*., **7,** 1499; (*b*) Gil, L., and Gilli, J. M., 1998, *Phys. Rev. Lett*., **80,** 5742.